Supplementary Information

A Sequentially Responsive and Structure-transformable Nanoparticle with Comprehensively Improved 'CAPIR cascade' for Enhanced Antitumor Effect

Chenfeng Xu [a], Yu Sun [b], YulinYu [a], Mei Hu [a], Conglian Yang [a], Zhiping Zhang [a, c, d, *]

AUTHOR ADDRESS

[a] Tongji School of Pharmacy, Huazhong University of Science and Technology, Wuhan 430030, China

[b] Ningbo First Hospital, Ningbo 315010, China.

[c] National Engineering Research Center for Nanomedicine, Huazhong University of Science and Technology, Wuhan 430030, China

[d] Hubei Engineering Research Centre for Novel Drug Delivery System, Huazhong University of Science and Technology, Wuhan 430030, China

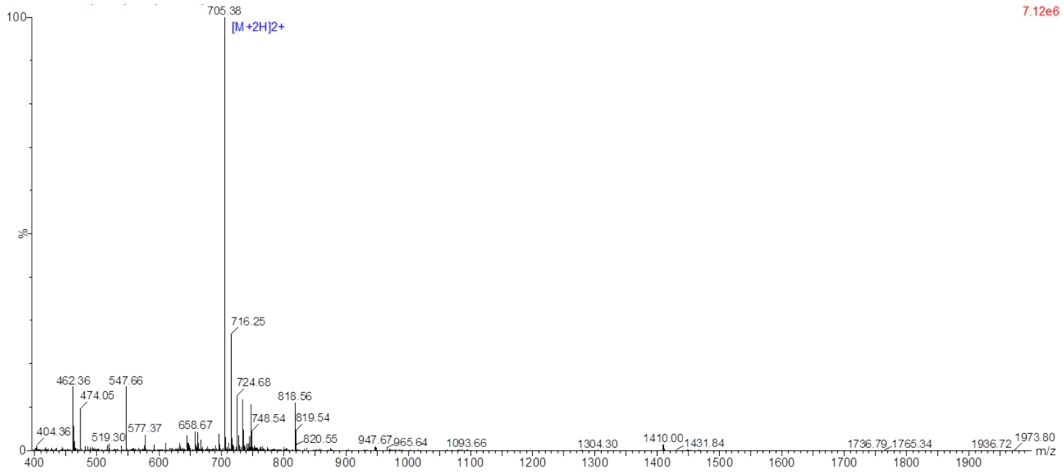

Fig.S1 The HRMS spectrum of 2-(Nap)-FFKAGLDD-RGD.

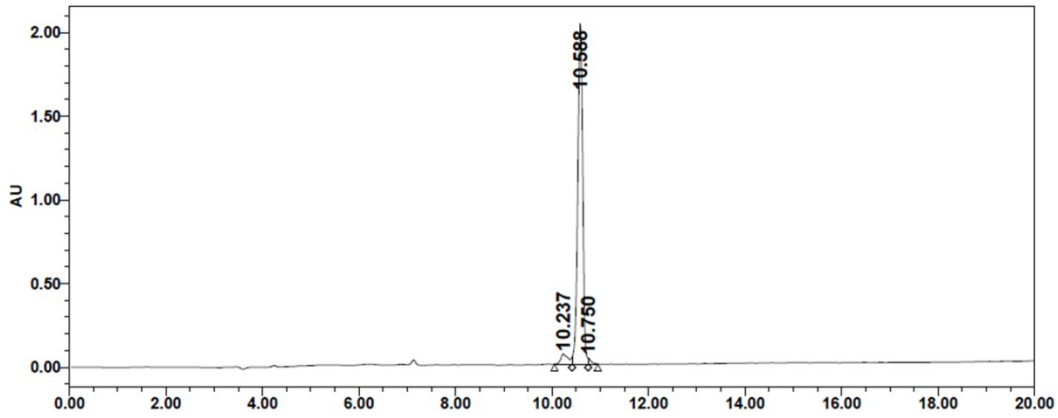

Fig.S2 The HPLC spectrum of 2-(Nap)-FFKAGLDD-RGD, purify is 94.76%.

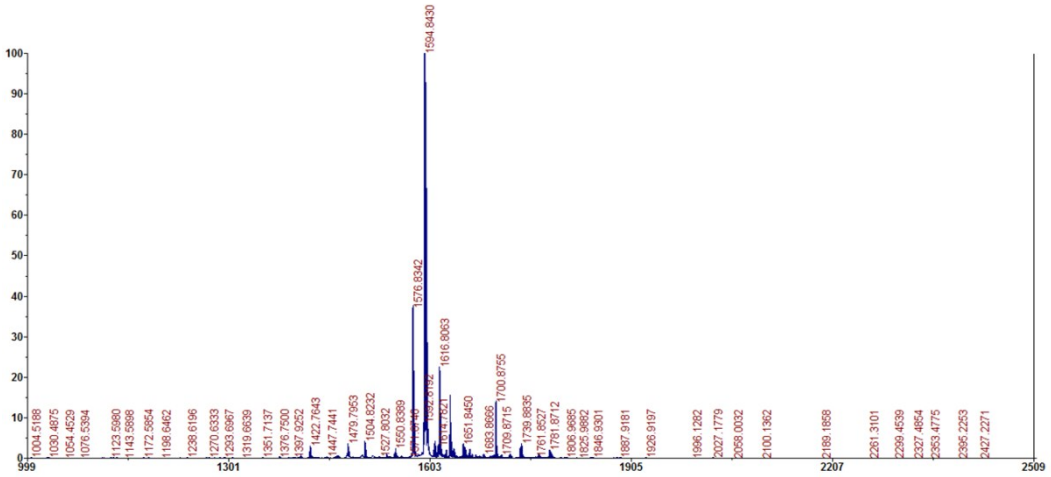

Fig.S3 The HRMS spectrum of 2-(Nap)-FFKWGLWD-RGD.

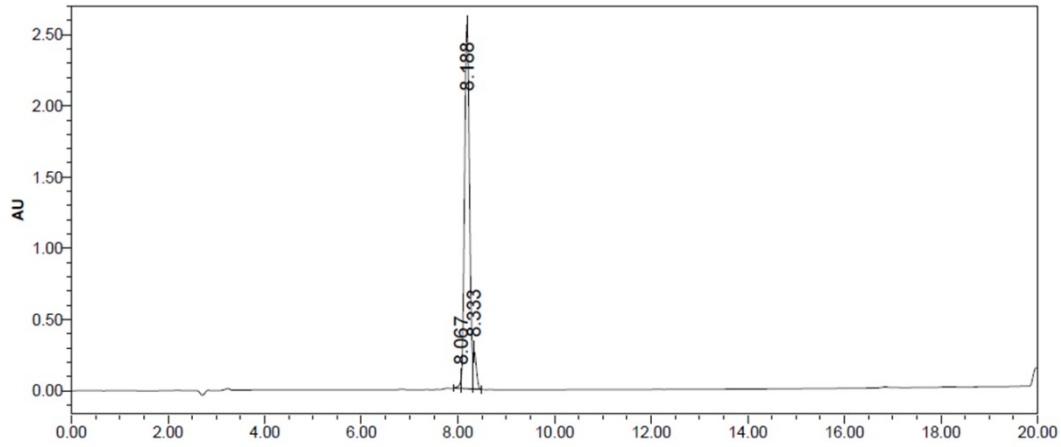

Fig.S4 The HPLC spectrum of 2-(Nap)-FFKWGLWD-RGD, purity is 93.37%.

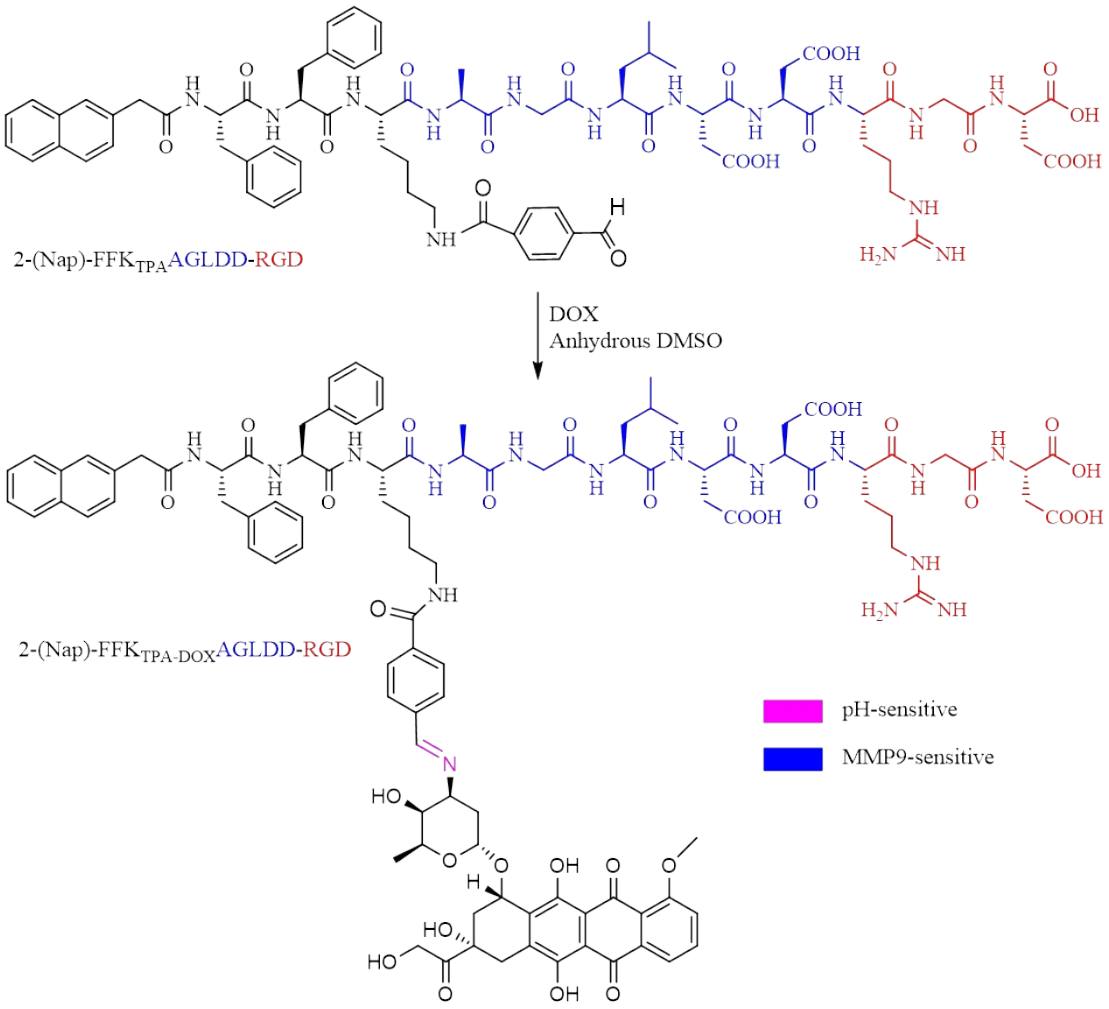

Fig.S5 Synthesis route of 2-(Nap)-FFK$_{TPA-DOX}$AGLDD-RGD (compound 1).

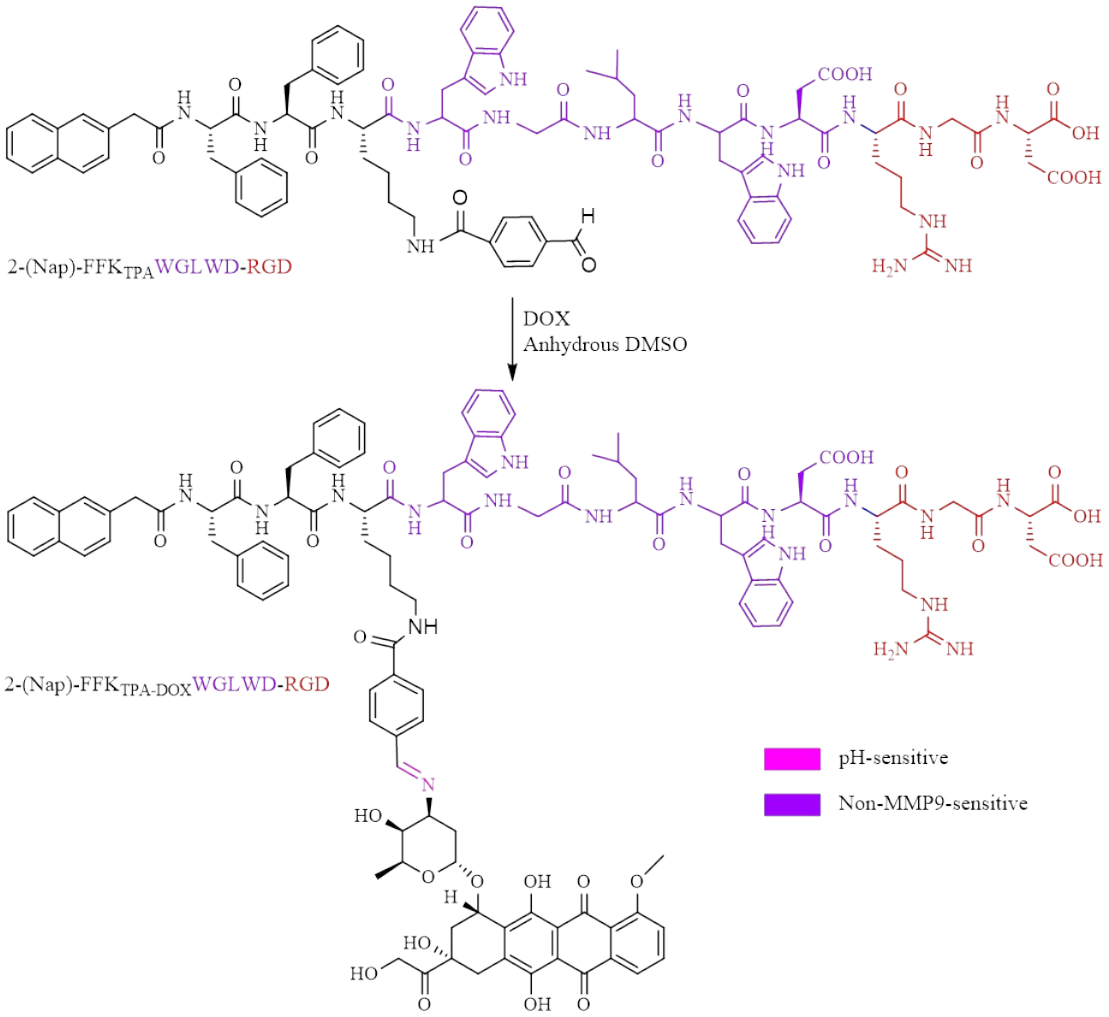

Fig.S6 Synthesis route of 2-(Nap)-FFK$_{TPA-DOX}$WGLWD-RGD (compound 2).

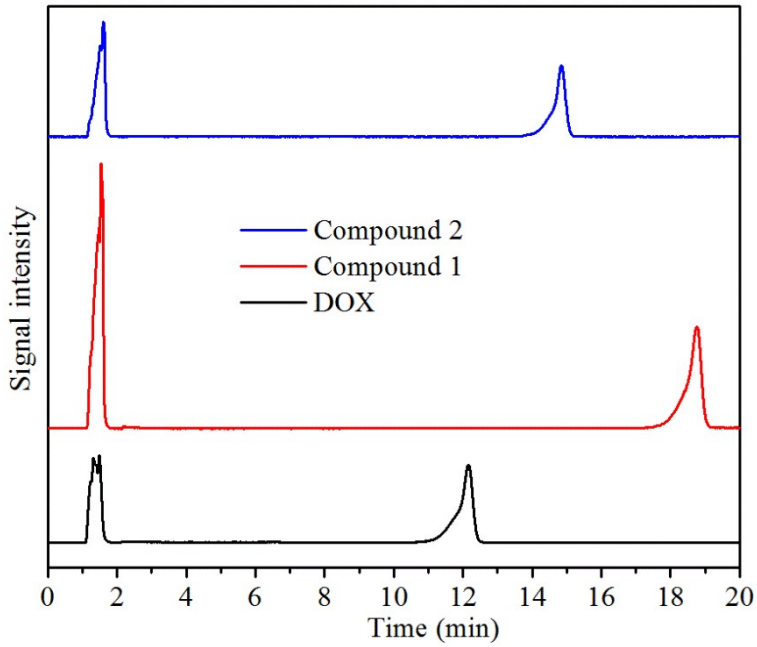

Fig.S7 The HPLC spectra of DOX, 2-(Nap)-FFK$_{TPA-DOX}$AGLDD-RGD (compound 1) and 2-(Nap)-FFK$_{TPA-DOX}$WGLWD-RGD (compound 2).

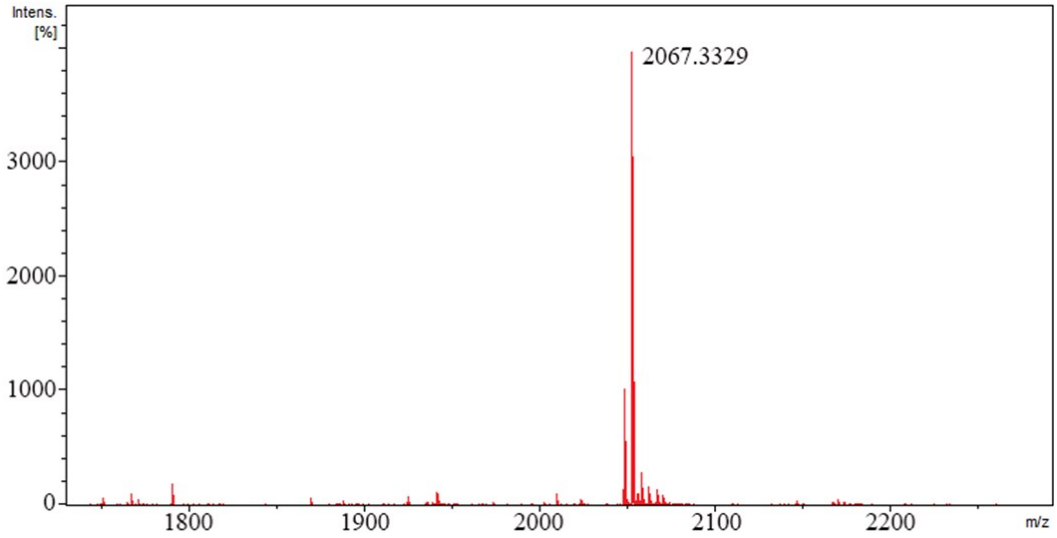

Fig.S8 The HRMS spectrum of 2-(Nap)-FFK$_{TPA-DOX}$AGLDD-RGD (compound 1).

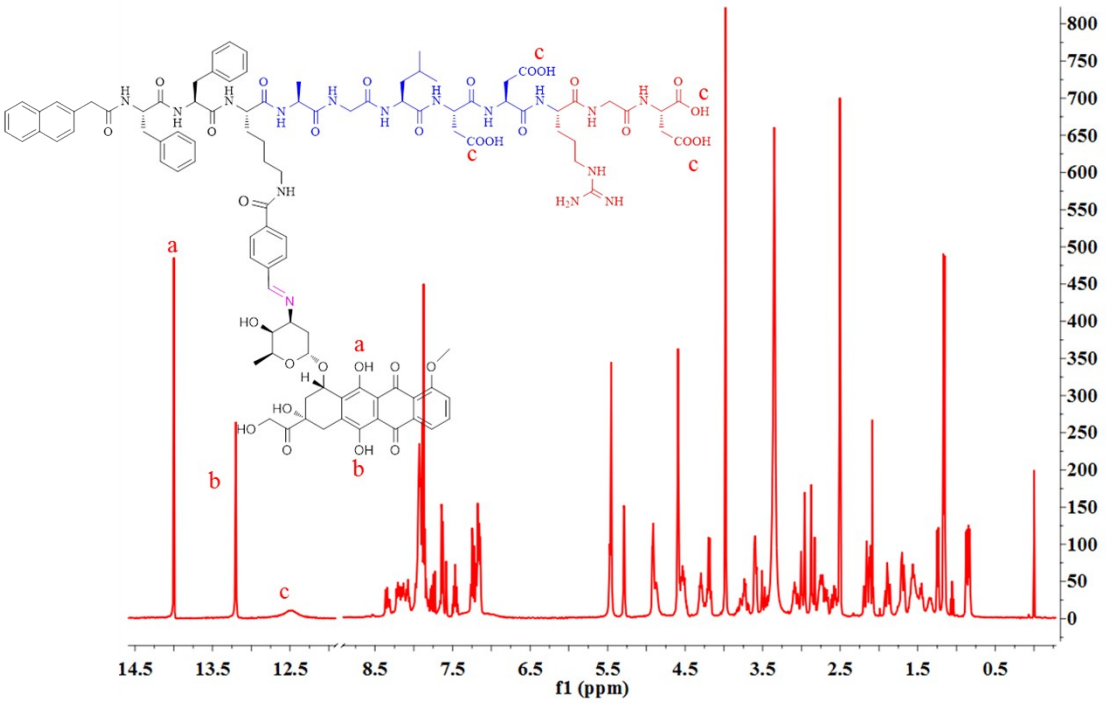

Fig.S9 The ^{1}H-NMR spectrum of 2-(Nap)-FFK$_{TPA\text{-}DOX}$AGLDD-RGD (compound 1, 400 MHz, *d6*-DMSO).

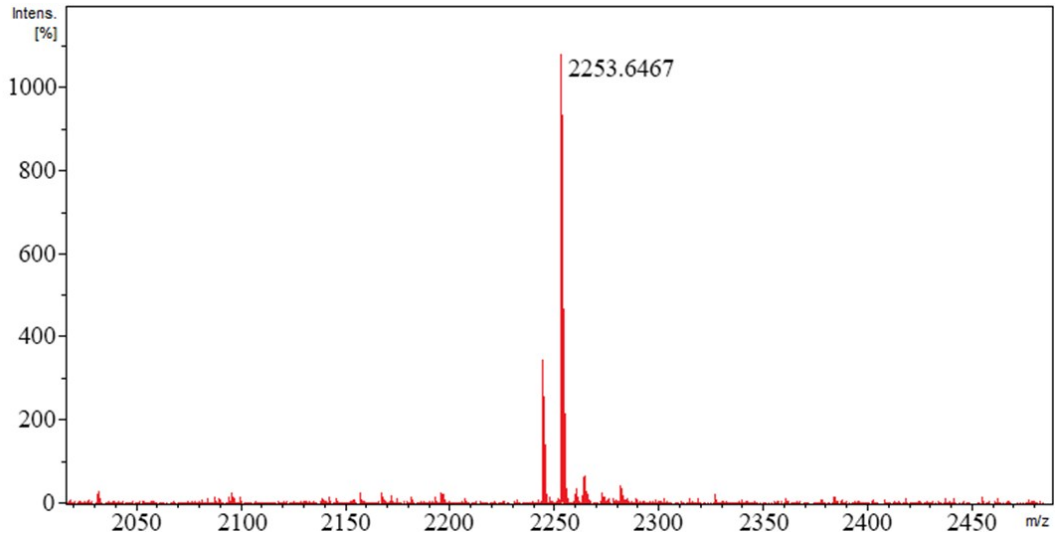

Fig.S10 The HRMS spectrum of 2-(Nap)-FFK$_{TPA\text{-}DOX}$WGLWD-RGD (compound 2).

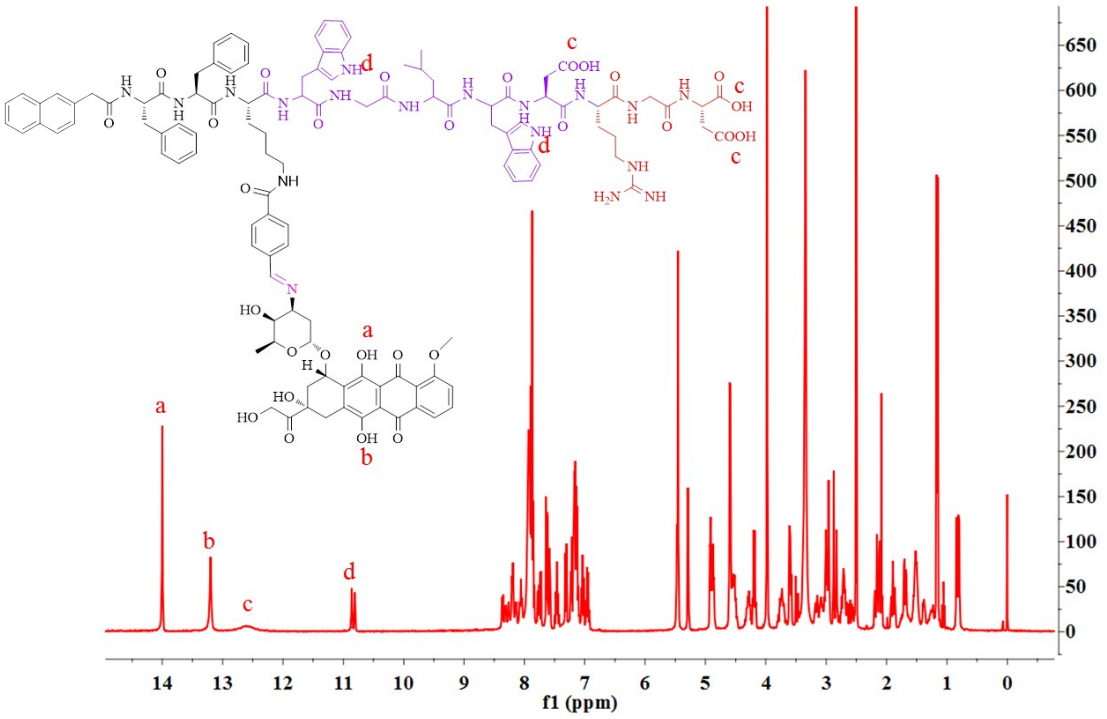

Fig.S11 The ^{1}H-NMR spectrum of 2-(Nap)-FFK$_{TPA\text{-}DOX}$WGLWD-RGD (compound 2, 400 MHz, *d6*-DMSO).

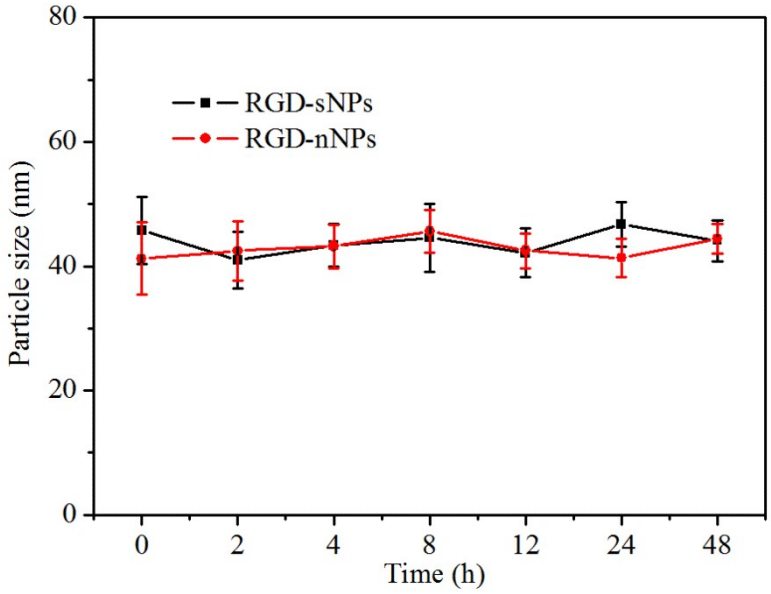

Fig.S12 The stability of RGD-sNPs and RGD-nNPs in PBS (pH7.4) containing 10% FBS at 37 °C for 48 h.

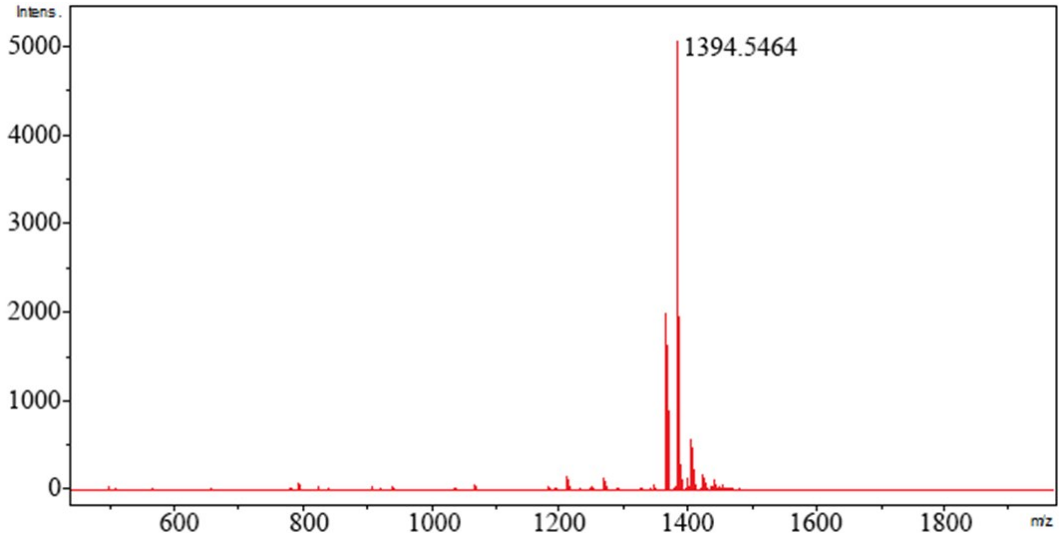

Fig.S13 The HRMS spectrum of intermediate generated from compound 1 that was treated for 12 h with MMP9, and the intermediate was determined as 2-(Nap) -$FFK_{TPA\text{-}DOX}AG$ according to the molecular weight, HRMS (ESI) m/z: ($[M+H]^+$) calcd for $C_{76}H_{79}N_7O_{19}$,1394.4760; found 1394.5464.

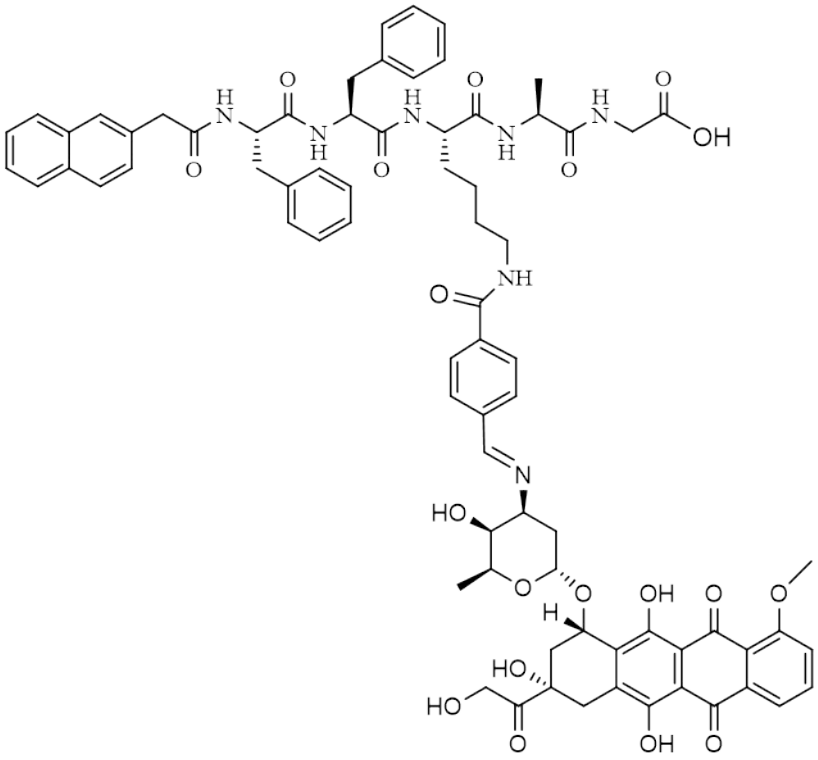

Fig.S14 The chemical structure of 2-(Nap)-$FFK_{TPA\text{-}DOX}AG$.

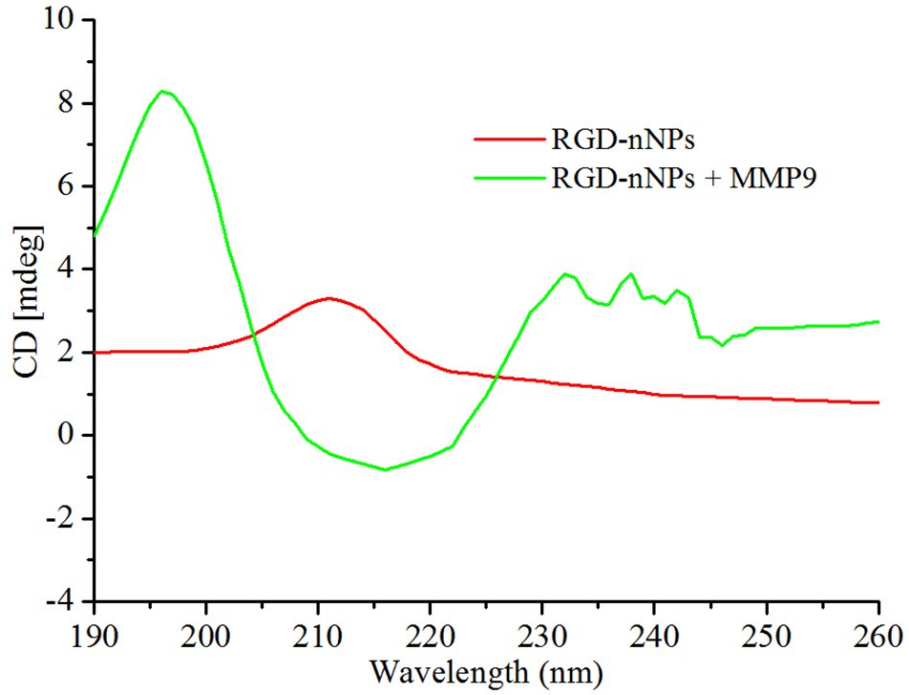

Fig.S15 The CD spectra of RGD-nNPs with or without MMP9 treatment.

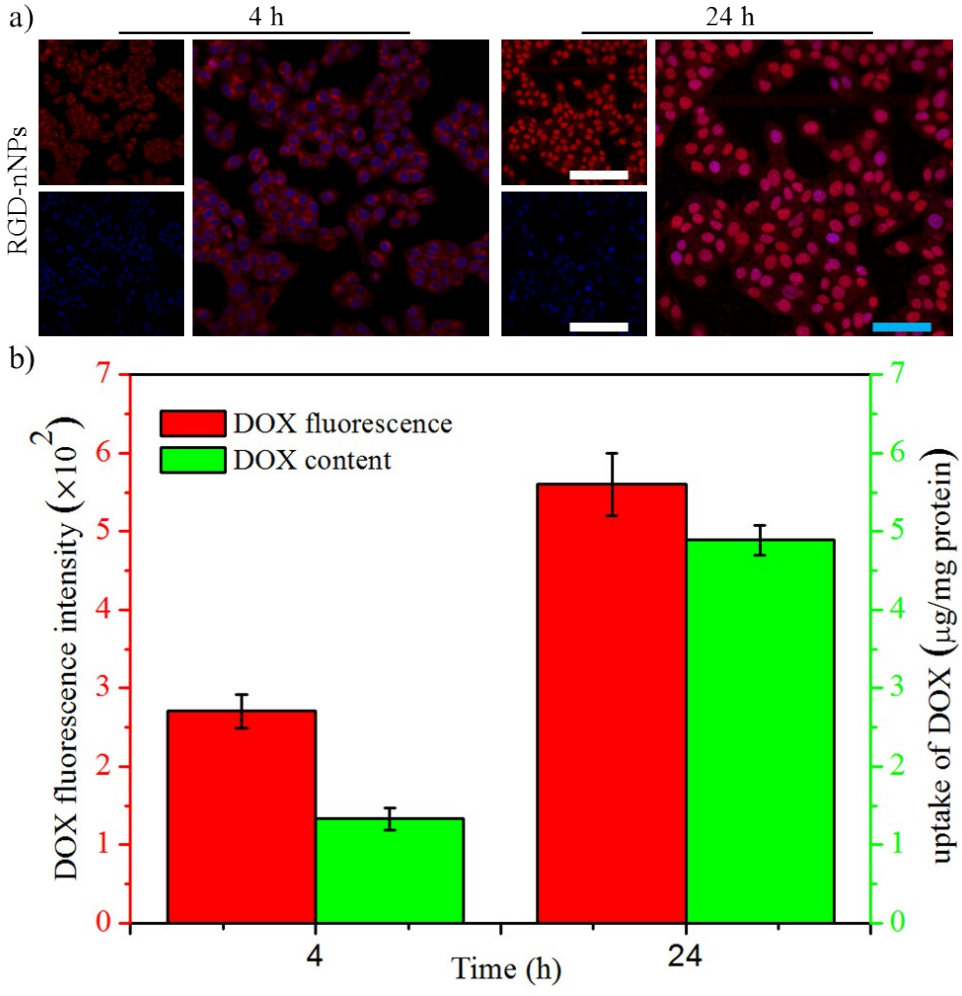

Fig.S16 Cellular uptake in HepG2 cells treated with RGD-nNPs. a) Confocal laser scanning microscope (CLSM) images of cellular uptake in HepG2 cells incubated with RGD-nNPs for 4 h or 24 h (white scale bar for 100 μm and blue scale for 50 μm), respectively. b) Quantitative analysis of DOX fluorescence intensity by flow cytometer and the amount of DOX internalized by HepG2 cells determined by HPLC (n=3).

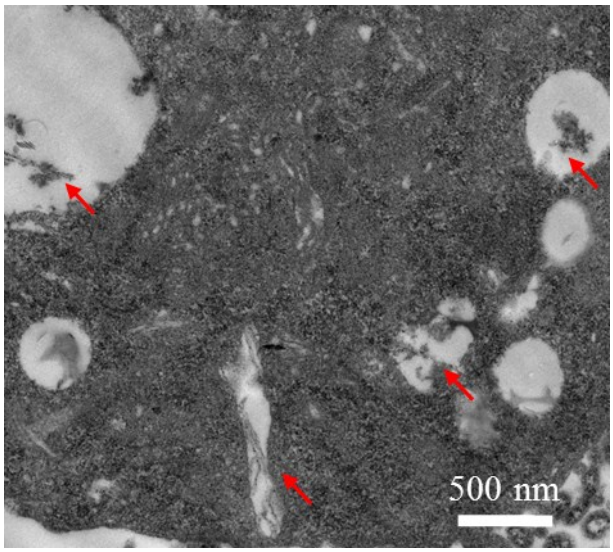

Fig.S17 Bio-TEM of HepG2 cells incubated with pretreated RGS-sNPs (pretreated MMP9 for 12 h) for 2 h (red arrows represent nanofibers in vessels or lysosomes).

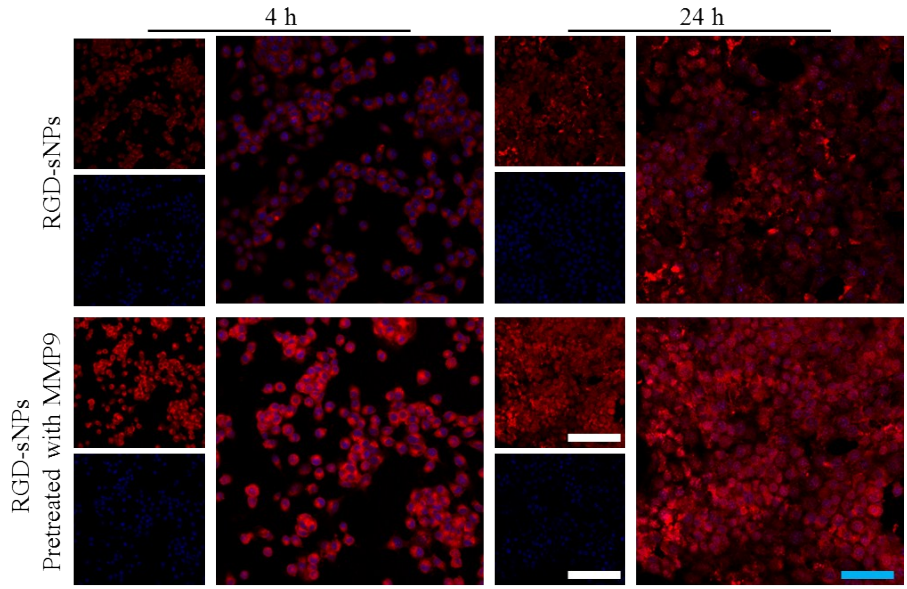

Fig.S18 Cellular uptake in 4T1 cells treated with RGD-sNPs or RGS-sNPs (pretreated MMP9 for 12 h) for 4 h and 24 h (white scale bar for 100 μm and blue scale for 50 μm), respectively.

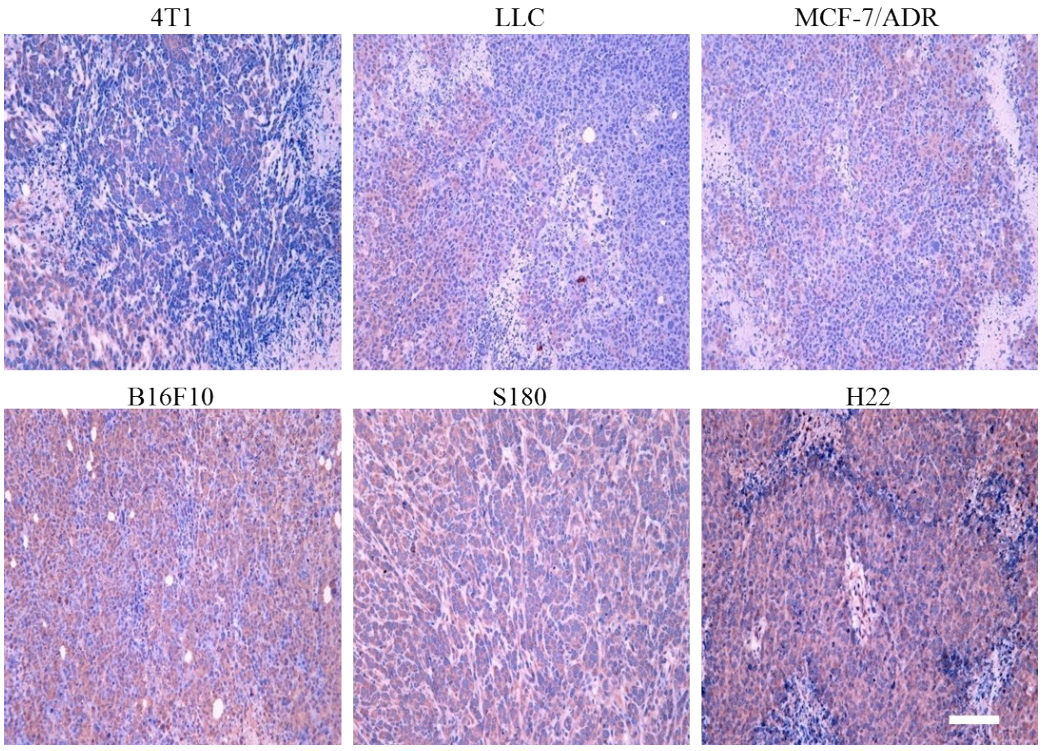

Fig.S19 The expression levels of MMP9 in different tumors as analyzed by immunohistochemical section (scale bar for 200 μm).

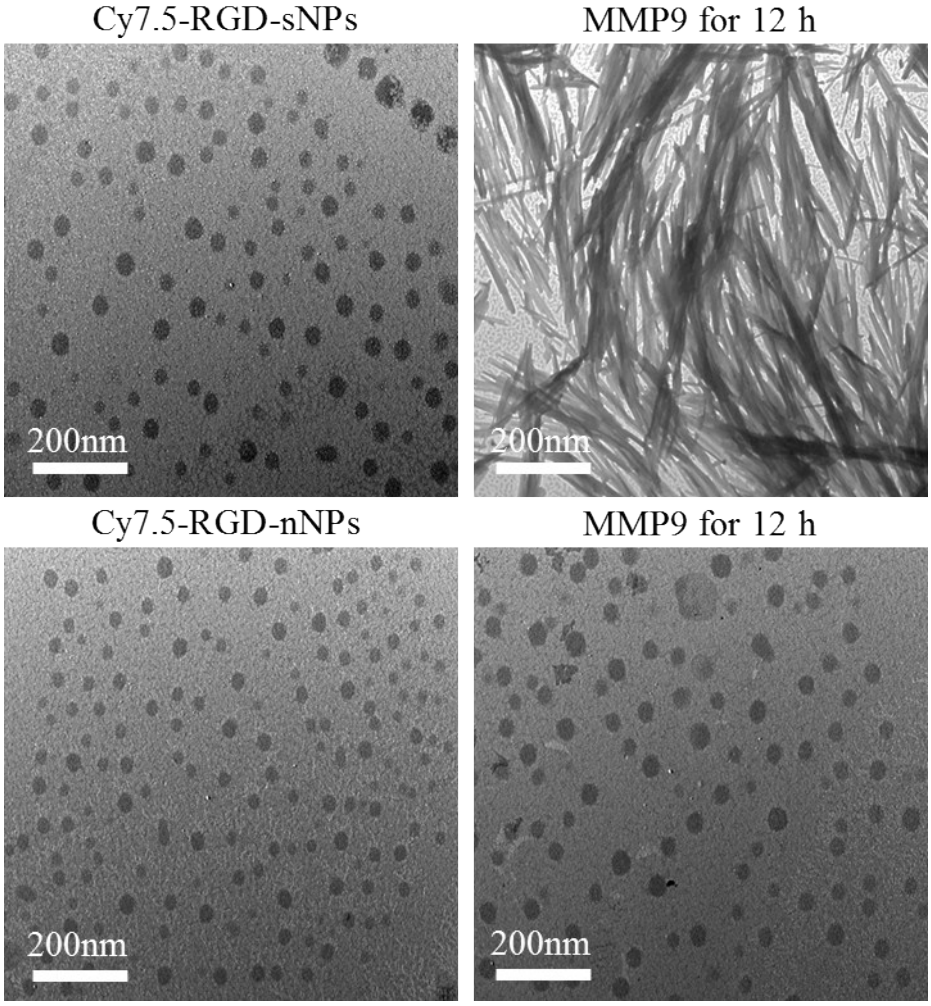

Fig.S20 The TEM images of Cy7.5-RGD-sNPs and Cy7.5-RGD-nNPs with or without MMP9 treatment.

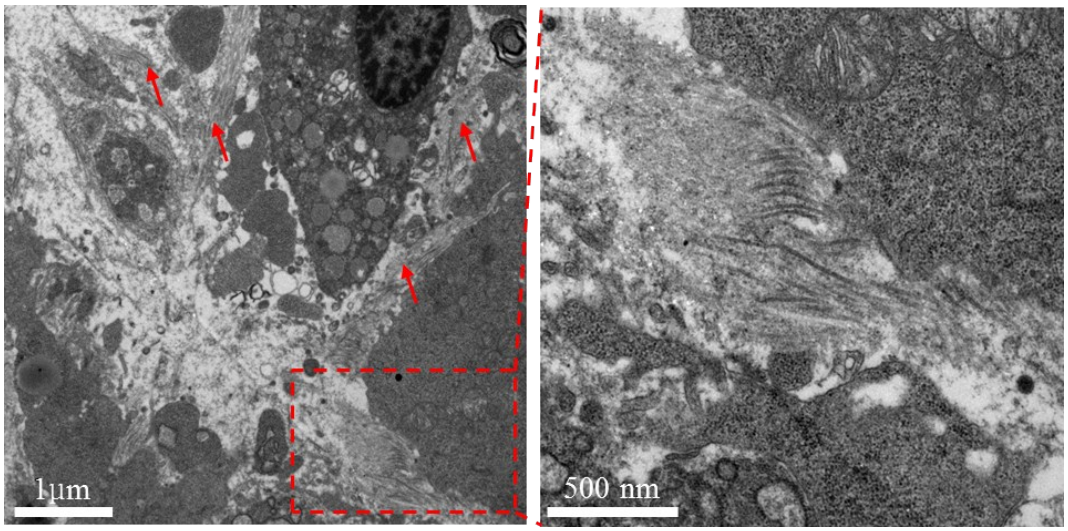

Fig.S21 Bio-TEM of in situ formed nanofibers in tumor region (red arrows represent nanofibers formed in tumor).

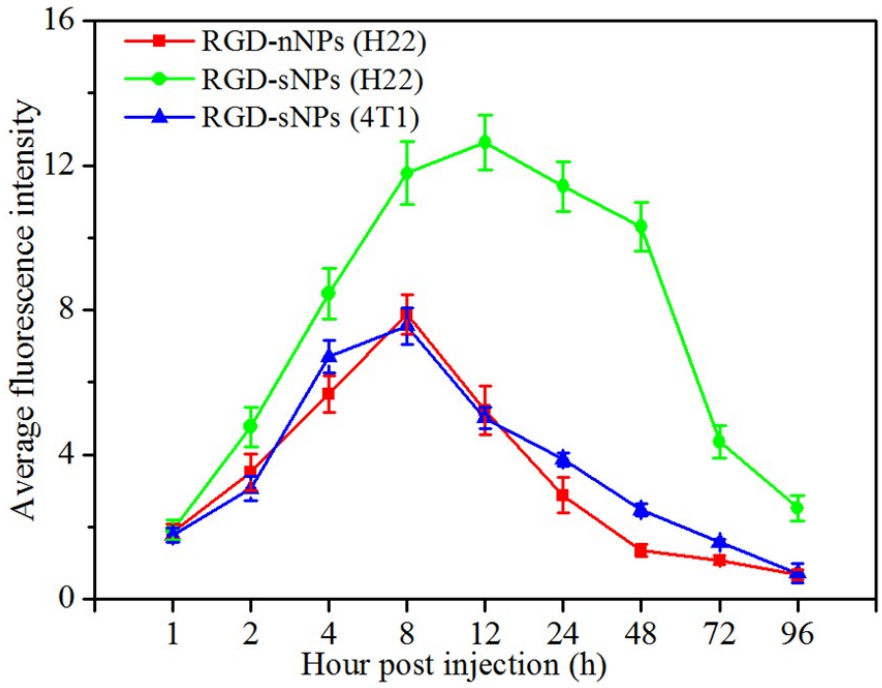

Fig.S22 The average fluorescence intensity in tumor region at different time point (n=3).

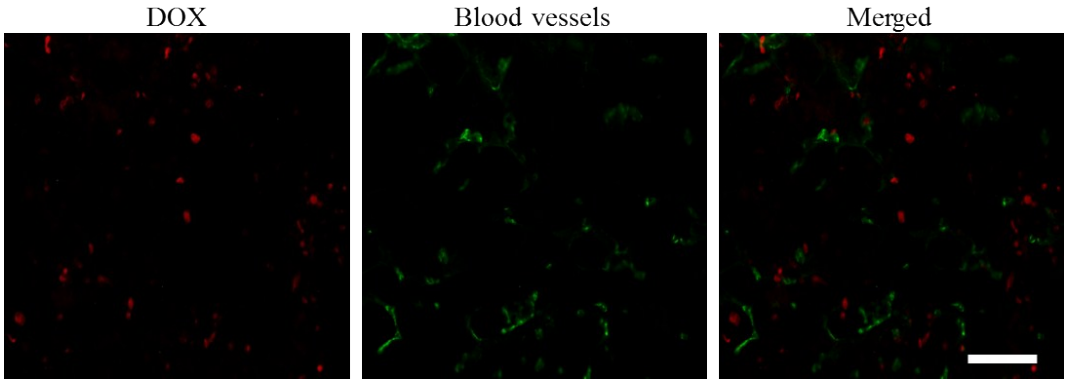

Fig.S23 *In vivo* penetration of DOX extravasated from blood vessels after intravenous injection of DOX solution for 48 h at DOX dose of 2.5 mg/kg (scale bar for 100 μm).

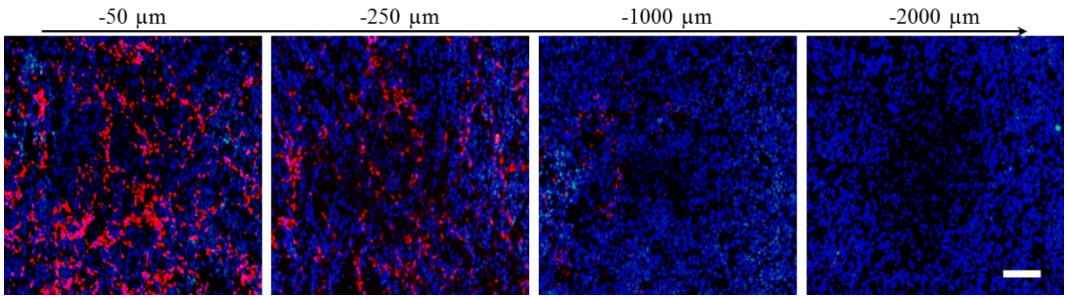

Fig.S24 *In vivo* penetration of DOX in tumors after intratumoral administration of DOX solution at DOX dose of 2.5 mg/kg for 48 h (scale bar for 100 μm). Frozen sections of tumors were sliced at different depths below the injection position.

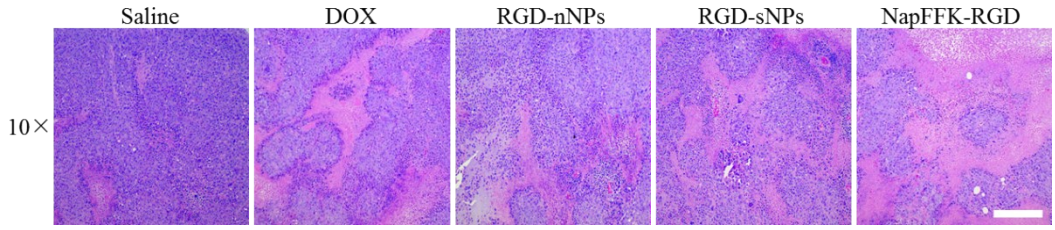

Fig.S25 The images of H&E for tumors resected from H22 tumor-bearing mice (scale bar for 200 μm).

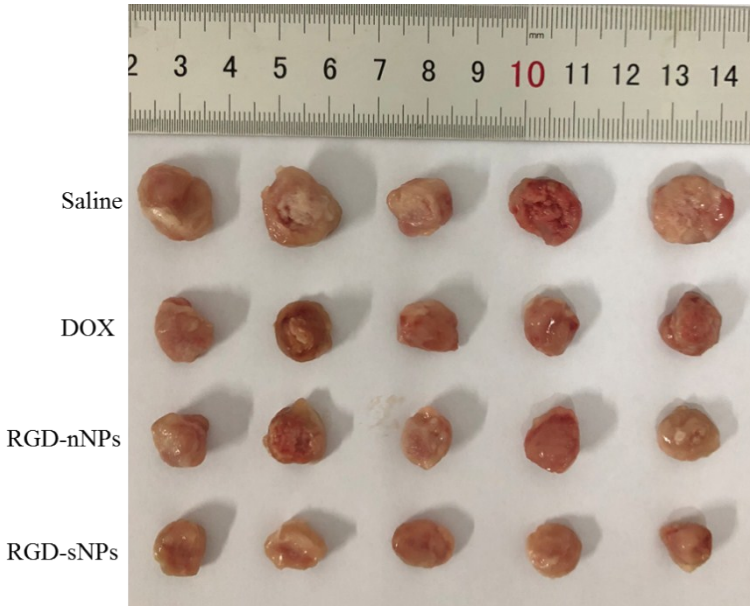

Fig.S26 The image of tumors (5/8) collected from 4T1 tumor-bearing mice after last treatment. The other three were stored at -80 ℃ after excision.

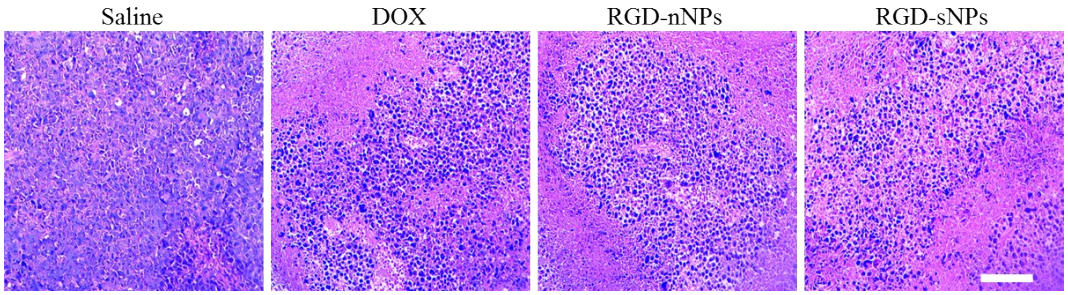

Fig.S27 The images of H&E for tumors resected from 4T1 tumor-bearing mice (scale bar for 100 μm).

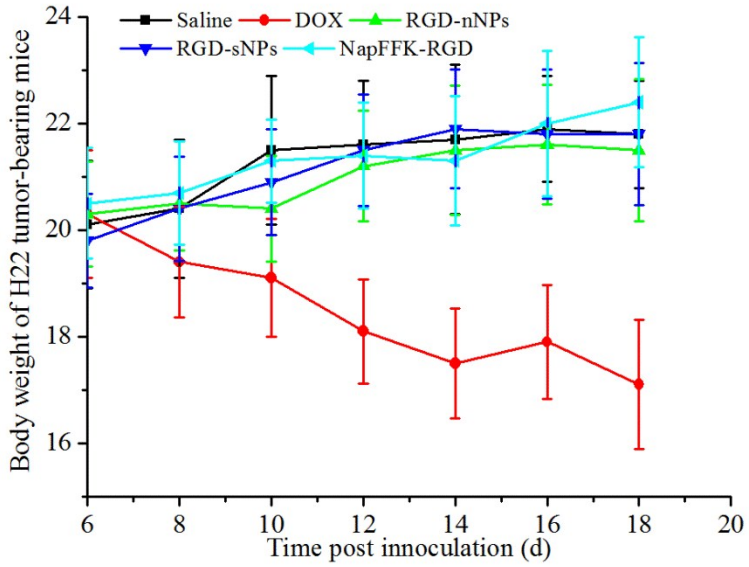

Fig.S28 The body weight change of H22 tumor-bearing mice (n=8).

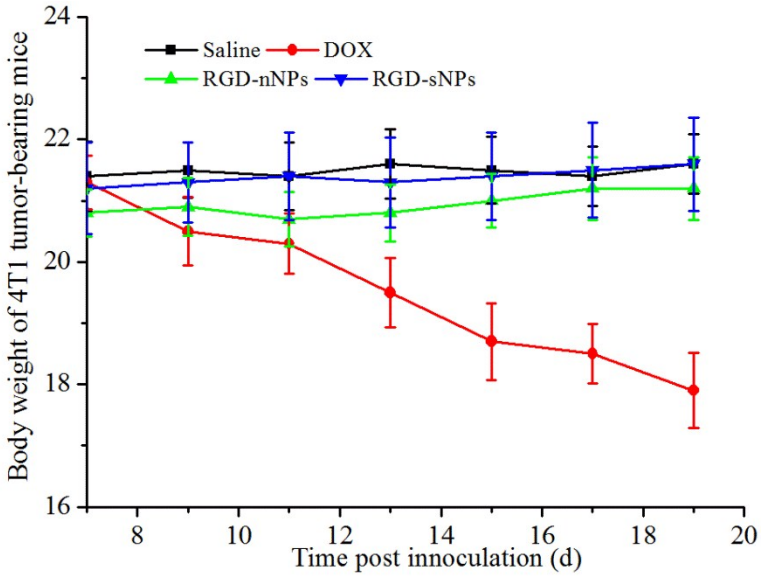

Fig.S29 The body weight change of 4T1 tumor-bearing mice (n=8).

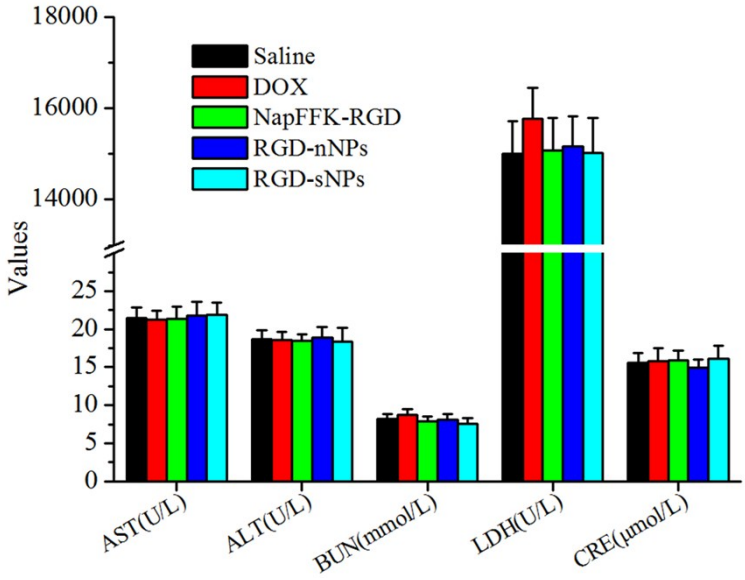

Fig.S30 The hematologic and biochemical parameters of plasma from H22 tumor-bearing mice (n=8).

Table S1 The IC_{50} values against L929 cell line after 48 h treatment (n=6).

Groups	IC_{50} values (μg/mL)[a)]
	L929
RGD-nNPs	504.25
RGD-sNPs	493.44

a) The half maximal inhibitory concentration.